Processes Determining the Rapid Reestablishment of the Equatorial Pacific Cold Tongue/ITCZ Complex

BIN WANG AND XIOUHUA FU

Department of Meteorology and International Pacific Research Center, School of Ocean and Earth Science and Technology, University of Hawaii at Manoa, Honolulu, Hawaii

(Manuscript received 11 February 2000, in final form 15 August 2000)

ABSTRACT

The annual reestablishment of the equatorial cold tongue (ECT) in the Pacific is signified by a remarkably rapid reversal of the warming trend from March to May. The processes responsible for this dramatic turnabout are investigated using the outputs generated by a coupled ocean–atmosphere model, which simulates realistic tropical Pacific climate. A new diagnostic equation is put forward for a budget study of the temperature tendency in a mixed layer (ML) with a variable depth. The budget study reveals that the rapid boreal spring cooling in the ML of the ECT (4°S–2°N, 120°–90°W) is primarily attributed to turbulent entrainment (54%), surface evaporation (21%), and meridional advection (14%). The spring shallowness of the ML is also a significant ''implicit'' contributor. Annually, the ML depth in the ECT varies nearly 180° out of phase with the SST while in phase with the ML heat content. The annual variation of the ML depth is determined by competing effects of the Ekman transport and turbulent entrainment. From March to July, the increase of the meridional wind component dominates that of the zonal component; thereby, the effect of entrainment surpasses that of upwelling, leading to mixed layer deepening. The mechanism governing the annual variation of the ML heat content is essentially the same as those governing the ML depth variation. The results suggest that accurate modeling of the ML turbulent mixing holds the key to realistic simulation of the annual cycle of the ECT.

In contrast, beneath the ITCZ (8°–12°N, 100°–120°W), the rapid spring warming is attributable to increased surface heat flux, while entrainment and thermal advection play minor roles. From February to May, the downward shortwave radiation and the surface latent heat fluxes, along with concurrent equatorial cooling, result in a northward progression of the annual warming and promote an active ITCZ–ECT interaction (including evaporation–wind feedback and cloud–radiation–SST interaction).

1. Introduction

In the equatorial eastern Pacific, the sea surface temperature (SST) reaches its height in March. From March to May, the equatorial cold tongue (ECT) in the Pacific rapidly cools, while the intertropical convergence zone (ITCZ) intensifies and moves northward. This is a period of dramatic seasonal change of the ITCZ–ECT complex. The annual variation of the atmospheric circulation in the eastern North Pacific (90°–120°W and 5°–15°N) exhibits characteristics of a typical monsoon (Murakami et al. 1992). The cause of the rapid reestablishment of the ECT from March to May and the sudden northward shift of the ITCZ along 100°W in May remains a controversial issue.

Mitchell and Wallace (1992) suggested the importance of the American monsoon in the annual cooling of the ECT. The onset of the summer monsoon over Colombia and Panama may intensify the surface southerlies over the eastern Pacific, which, in turn, brings colder water up to the surface. Using an anomaly-coupled ocean–atmosphere model, Chang and Philander (1994) and Chang (1996) demonstrate how the intensifying southerlies cause the upwelled cold water appearing south of the equator and then advect the cold water to the equator, reestablishing the cold tongue. Their model assumed a mixed layer (ML) with a constant depth. Thus, upwelling acts directly to change SST, and the Ekman dynamics and meridional advection by currents play key roles in the annual cooling of the ECT. By diagnosing results obtained from an ocean model developed by Chen et al. (1994), Kessler et al. (1998) concluded that the most important factors responsible for the spring sea surface cooling are the intensified upwelling and surface latent heat flux. Note that Kessler et al. also assumed a constant ML depth. Because the magnitude of the annual variation of observed ML depth in the equatorial eastern Pacific is as large as its mean (Kesseler et al. 1998; Swenson and Hanson 1999), it is essential to assess the role of the ML depth variation in the annual cycle of ECT and further explore the causes of the annual variation of the ML depth.

Corresponding author address: Dr. Bin Wang, Department of Meteorology, University of Hawaii, 2525 Correa Road, Honolulu, Hawaii 96822.
E-mail: bwang@soest.hawaii.edu

© 2001 American Meteorological Society

A central question to be addressed in the present paper is: what oceanic and surface exchange processes cause the rapid annual reestablishment of the cold tongue and associated northward SST gradients between the cold tongue and the ITCZ? The answer to this question holds the key to an understanding of the onset of the eastern North Pacific summer monsoon. To address this question, our strategy is to use output obtained from numerical integration of a coupled ocean–atmospheric model with an intermediate level of complexity. Use of coupled ocean–atmosphere model output for diagnostic studies has its advantage compared with the use of a stand-alone ocean model. The present flux climatology, numerical weather prediction model flux fields, and satellite products exhibit considerable inconsistencies. This is particularly true in the eastern Pacific (Yu and McPhaden 1999). The possible distortion of the ocean heat balance due to errors in the forcing fields is unknown. On the other hand, in coupled models, the flux exchanges are determined internally within the coupled system. If the coupled models reproduce realistic annual cycles in both the ocean and atmosphere, the diagnostics based on the outputs from the coupled models may provide physically consistent results and useful physical insights.

In section 2, we first compare the model's simulation of the annual march of the ITCZ–ECT complex with available observations. Section 3 presents a diagnostic framework for understanding SST variation and ML heat budget. This new scheme allows identification of the contributions from each individual physical process without assuming a constant mixed layer depth. The processes responsible for the rapid establishment of strong meridional SST gradients between the ECT and the ITCZ are then diagnosed. The diagnoses focus on revealing the processes that determine the annual reestablishment of the cold tongue (section 4) and the annual variation of the mixed layer depth (section 5), and the northward progression of annual warming from the ECT to ITCZ (section 6). Last, a summary is given and the role of air–sea interaction in the annual reestablishment of the ECT–ITCZ complex is discussed.

2. Simulated seasonal march of the ITCZ–ECT complex

The coupled model used in this study is described in detail in Fu and Wang (2001). For the reader's convenience, a brief summary is provided here. The atmospheric component of the model is a 2.5-layer primitive equation model on the equatorial beta plane (Wang and Li 1993; Fu and Wang 1999). It emphasizes the interactions between heating-forced free troposphere flows and SST gradient–forced boundary layer flows. The model atmosphere covers the global Tropics between 30°S and 30°N. The standard horizontal resolution is 2° lat × 4° long. The ocean component is a modified version of Wang et al. (1995). It comprises a mixed layer and a thermocline layer. The primitive dynamic equations are used for both layers. A primitive thermodynamic equation is used in the mixed layer. A self-contained subsurface temperature scheme is introduced to represent the entrained water temperature. The entrainment rate at the mixed layer base is estimated with the turbulent parameterization of Gaspar (1988). The ocean model extends from 30°S to 30°N and 120°E to 80°W with realistic but simplified east and west boundaries of the Pacific Ocean. The atmosphere and ocean are actively coupled in the Pacific Ocean region with interfacial fluxes and SST exchanged once per day. At the north and south boundaries of the ocean model, heat flux correction is used to relax the model SST back to the observed temperature. This correction is applied only poleward of 20°S and 20°N. Outside of the Pacific region, the surface temperature forcing the atmosphere is specified to be the observed SST over ocean and the 1000-hPa air temperature from the European Centre for Medium-Range Weather Forecasts analysis over land. To reduce errors in the interface heat exchanges, we used climatologically monthly cloud cover from the International Satellite Cloud Climatology Project (ISCCP) observations to calculate the ocean surface radiative heat fluxes and atmospheric longwave radiation. This intermediate coupled model reproduces the climatological mean and annual cycle of the tropical Pacific (e.g., surface winds, rainfall, SST, oceanic currents) well. The detailed formulation of this model and its performance have been presented in Fu and Wang (2001). Here, we focus on the model's simulation of the ITCZ–ECT complex.

The annual cycle of the ITCZ–ECT complex exhibits a predominant latitudinal variation that can be conveniently illustrated using meridional (along 100°W) cross sections of the SST, surface winds, and precipitation (Fig. 1). The SST reaches its annual maximum in March–April near the equator and progressively later northward in both the observations and simulations. The observed equatorial SST reaches a minimum during September and October (Fig. 1a). The minimum SST is captured by the model, although the minimum is slightly higher than its observed counterpart (Fig. 1e). The zone of coldest water centered at 2°S is primarily caused by the cross-equatorial southerlies, which induce upwelling just to the south of the equator caused by a sharp decrease in the Coriolis effect near the equator (Chang and Philander 1994). The simulated annual cycle of the zonal winds associated with the eastern North Pacific Summer Monsoon in the Northern Hemisphere is too weak and the observed westerly maximum in June is missed (Figs. 1b and 1f). In both the observation and the simulation, the southerlies between the equator and 5°N are weakest in March, and rapidly intensify from March to June in association with the annual cooling of the ECT (Figs. 1c and 1g). The northward movement and intensification of the ITCZ rainfall from March to June are simulated reasonably well, as is the maximum rainfall that occurs in June and July around 8°N (Figs. 1d and 1h). However, the model

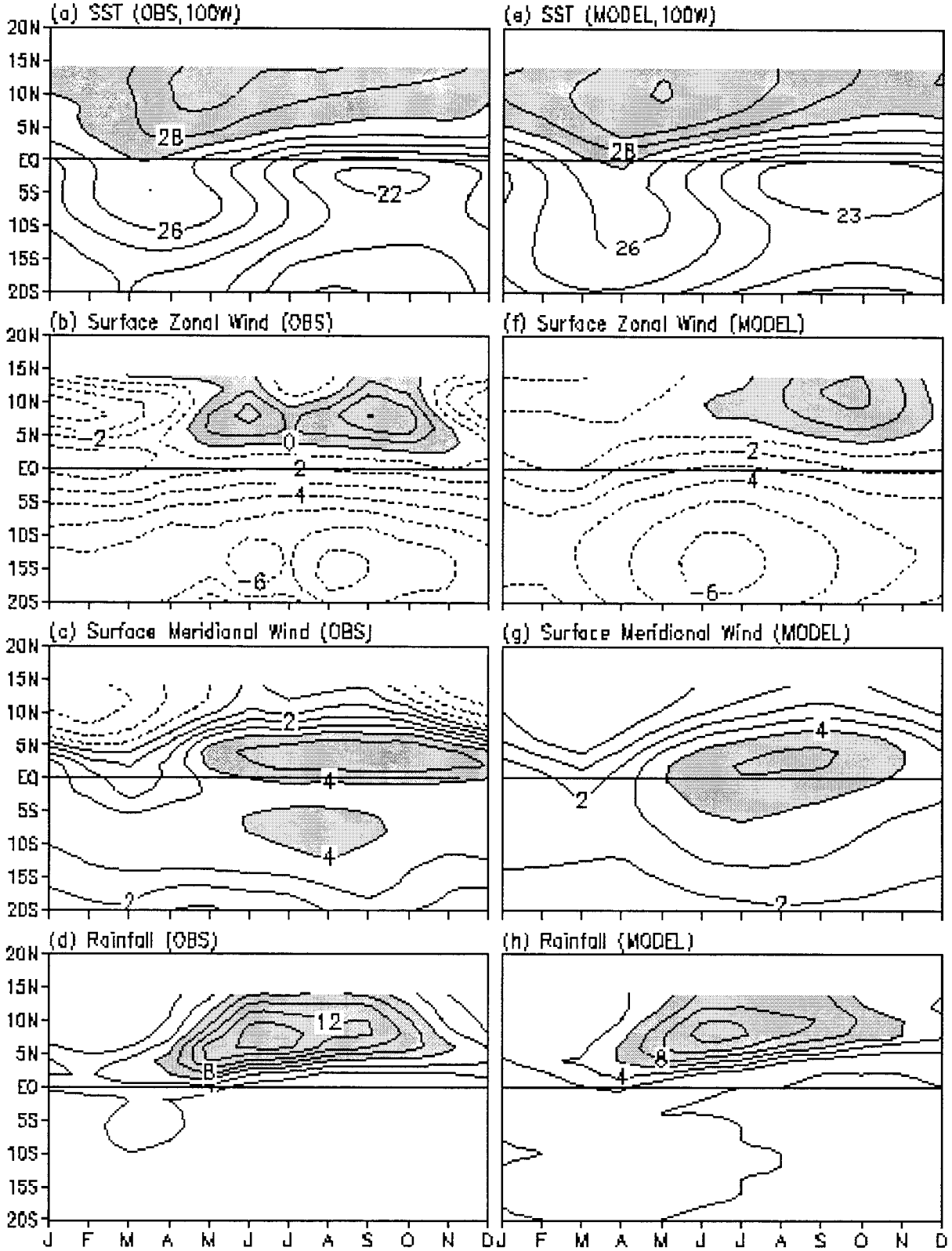

FIG. 1. The (left) observed and (right) simulated annual variations of (a), (e) SST, (b), (f) surface zonal wind, (c), (g) surface meridional wind, and (d), (h) rainfall along 100°W. The observed surface winds and precipitation were derived, respectively, from COADS compiled by Sadler et al. (1987) and the Climate Prediction Center (CPC) merged analysis of precipitation (Xie and Arkin 1996).

performs poorly in simulating the equatorward retreat of the ITCZ from October to January. This deficiency is related to the missing northerlies north of the ITCZ in the model (Fig. 1g).

Our diagnostic analysis will focus on the ECT and associated ITCZ. Therefore, particular attention is given to the model's performance in these two regions. To represent the ECT, Kessler et al. (1998) defined a rectangular area from 4°S to 2°N and from 120° to 90°W. The ITCZ in the eastern Pacific will be represented by the rectangular region stretching from 8° to 12°N and from 120° to 100°W. This box reflects the summer mean location of the ITCZ north of the ECT. The observed ML depth is defined to be the depth at which the subsurface water temperature differs from the SST in the same vertical column by 1°C. Observed ML currents were obtained by vertically averaging the currents within the mixed layer.

In the ECT, the simulated annual variations of the SST, ML depth, and ML zonal currents resemble their observed counterparts (Fig. 2). The decrease of SST from April to June is reasonably well simulated (Fig. 2a). The ML is shallowest in March (Fig. 2b) in association with light surface winds and large downward surface heat fluxes, which act to reduce the ML base entrainment rate. The opposite condition occurs in late summer to early autumn. The ML zonal currents are primarily driven by the zonal component of the surface winds. Weak (strong) easterly winds in spring (late summer) are responsible for the weak (strong) westward currents. The simulated annual variation of the surface wind speed is reasonable but is excessively strong from April to August (Fig. 2d).

Around 10°N, the amplitude and phase of the simulated annual variation of SST agrees well with observations. However, there is a systematic warm bias (Fig. 3a). From January to May, the ocean under the ITCZ warms up rapidly, followed by a gradual cooling during the rest of the year. The observed ML depth exhibits an apparent semiannual cycle with a moderate amplitude (Fig. 3b). The simulated ML depth is dominated by an annual harmonic with amplitude larger than that observed. The simulated and observed annual mean depths are nearly the same. As shown in Fig. 1, the northeasterly winds north of the ITCZ in late winter and early spring are not well reproduced. The shallow ML during this period reflects the errors in the simulated wind speed. The phase of the simulated zonal currents compare favorably with the corresponding observations, but the amplitude of the annual variation is substantially underestimated (Fig. 3c). The simulated annual variation of the rainfall rate in the ITCZ agrees well with observations except that the amplitude is underestimated (Fig. 3d). Both the observed and simulated annual variations of ITCZ rainfall show a rapid increase from March to June. The intensification of ITCZ rainfall is associated with the warming under the ITCZ and the cooling of the ECT.

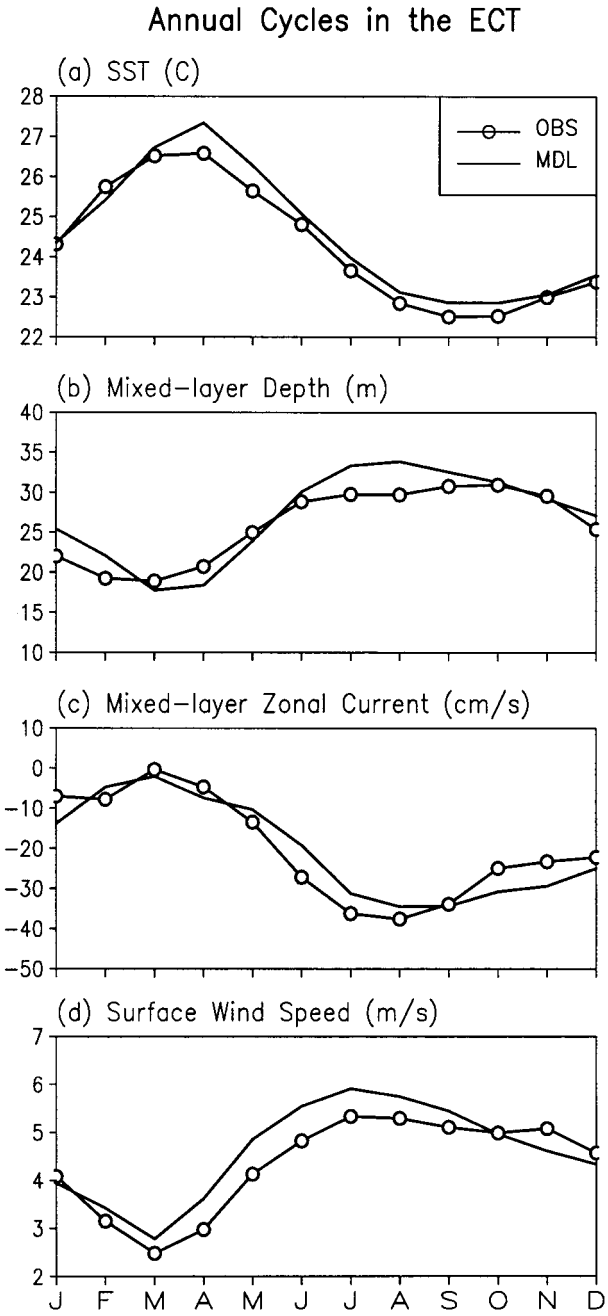

FIG. 2. Annual variations of the observed and simulated (MDL) (a) SST, mixed layer (b) depth and (c) zonal currents, and (d) surface wind speed in the equatorial cold tongue of the eastern Pacific (4°S–2°N, 120°–90°W). The data derived from the Ocean Data Assimilation System at the National Centers for Environmental Prediction (Ji et al. 1995) are used to represent the observations.

The meridional winds and SST difference between the ITCZ and ECT increase rapidly from March to May, following the annual cooling of the ECT and the warming in the ITCZ (Figs. 4a,b). Both the observations and the model show maximum warming in the ITCZ (+0.8°C) from March to April (Table 1) and maximum cooling in

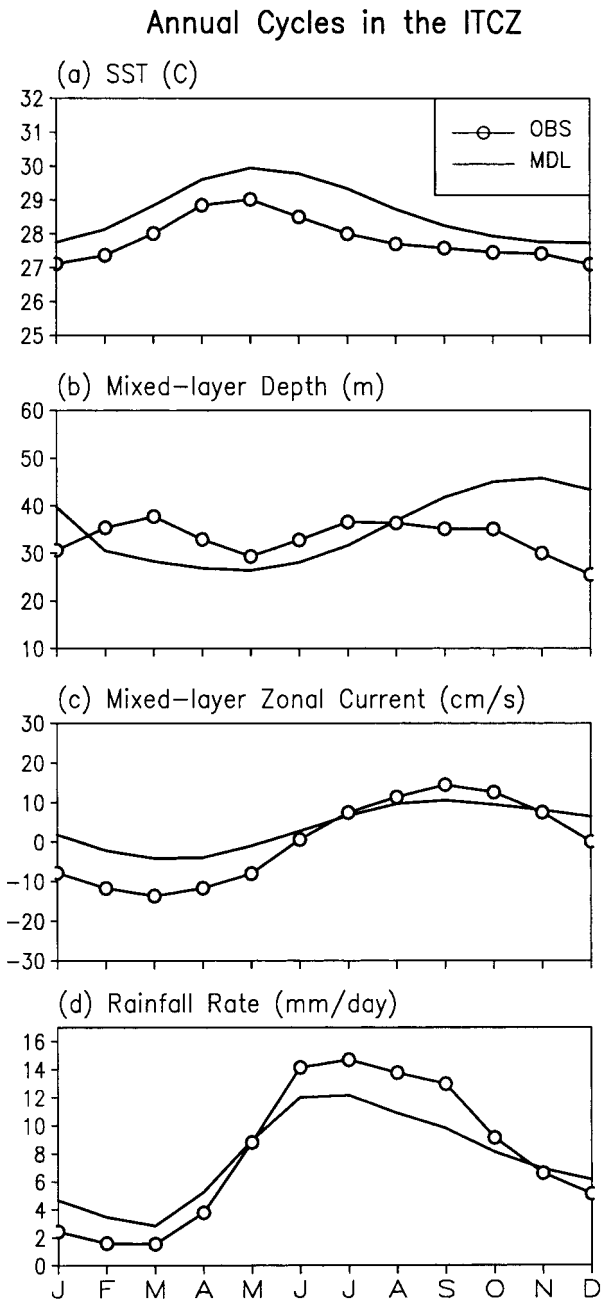

FIG. 3. Annual variations of the observed and simulated (MDL) (a) SST, mixed layer (b) depth and (c) zonal currents, and (d) rainfall rate in the ITCZ of the eastern Pacific (8°–12°N, 120°–100°W).

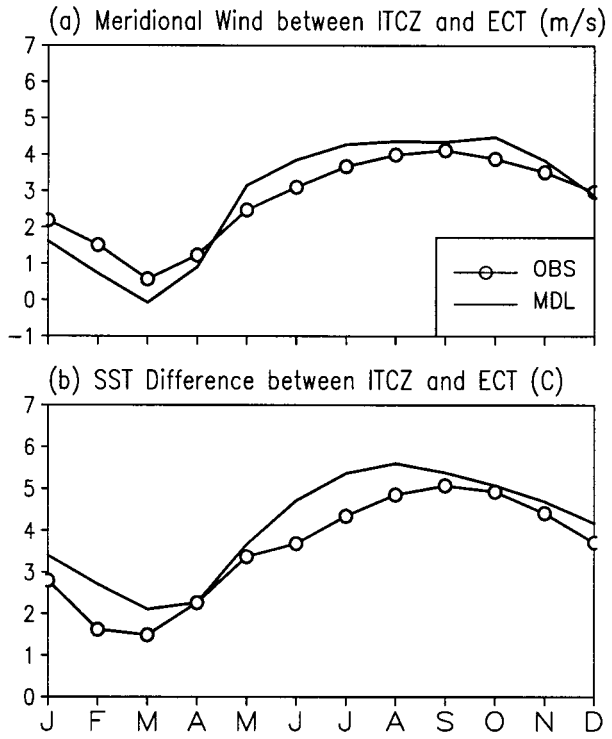

FIG. 4. Annual variations of the observed and simulated (MDL) (a) meridional winds and (b) SST difference (°C) between the ITCZ and ECT.

the ECT (about −0.8°C) from April to May (Table 1). The observed meridional SST difference between the ITCZ and ECT increases by +1.7°C from March to May, which is a result of the warming of the ocean under the ITCZ (+1.0°C) and the concurrent cooling of the cold tongue (−0.7°C). In the model, the corresponding SST difference increases by +1.4°C, primarily due to the warming of the ITCZ (+1.1°C). This discrepancy arises from the phase delay in the simulated sea surface cooling in the ECT from March to April (Fig. 2a). As a result, the buildup of the meridional SST gradient in the model occurs primarily from April to May.

In summary, the model's annual variations of the SST, rainfall, surface winds, and related ML depth and currents in the eastern Pacific are reasonably realistic. In particular, the agreement between the simulation and observations in spring (March, April, May) is good. This lends confidence to the following diagnostic analysis of the physical processes that govern the rapid changes of the SST in boreal spring and in the ITCZ–ECT complex.

3. Diagnostic framework

In previous studies, the ML heat budget has been based on the following thermodynamic equation applied to a vertical ML column (e.g., McPhaden 1982; Chen et al. 1994):

TABLE 1. Observed (OBS) and simulated (MDL) SST changes (°C) in the ITCZ and equatorial cold tongue (ECT) and the difference between ITCZ and ECT (ITCZ–ECT).

	ITCZ		ECT		ITCZ–ECT	
	OBS	MDL	OBS	MDL	OBS	MDL
Apr–Mar	+0.8	+0.8	+0.1	+0.6	+0.7	+0.2
May–Apr	+0.2	+0.3	−0.8	−0.9	+1.0	+1.2
May–Mar	+1.0	+1.1	−0.7	−0.3	+1.7	+1.4

$$\frac{\partial T_1}{\partial t} = \underbrace{-u_1\frac{\partial T_1}{\partial x}}_{(R_u)} \underbrace{- v_1\frac{\partial T_1}{\partial y}}_{(R_v)} + \underbrace{\frac{Q_{\text{ent}} + Q_{\text{nsw}} + Q_{\text{lh}} + Q_{\text{sh}} + Q_{\text{lw}}}{\rho_r C_w h_1}}_{(R_h)} + \underbrace{\mu\nabla^2 T_1}_{(R_d)}, \tag{3.1}$$

where

$$Q_{\text{ent}} = -\rho_r C_w W_e H(W_e)(T_1 - T_e)$$

denotes the entrainment heat flux at the ML base; h_1, T_1, u_1, v_1, and W_e are, respectively, the depth, temperature, vertical mean zonal and meridional currents of the ML, and the entrainment velocity at the ML base; ρ_r and C_w denote density and specific heat of the ML water, respectively; $H(W_e)$ is a Heaviside step function of W_e; T_e represents subsurface temperature that measures the entrained water, and μ is a horizontal heat diffusion coefficient; $Q_{\text{nsw}} = Q_{\text{sw}}|_{h=0} - Q_{\text{sw}}|_{h=-h_1}$ denotes the net shortwave radiation received by the mixed layer; Q_{lh}, Q_{sh}, and Q_{lw} represent downward latent heat, sensible heat, and net longwave radiation fluxes at the surface, respectively. In (3.1), the sign of each flux term is positive (negative) if it contributes to a ML heat gain (loss). The entrainment velocity is calculated based on the turbulent kinetic energy balance scheme (Gaspar 1988). The subsurface temperature is parameterized by temperature gradient in the model thermocline layer (Wang et al. 1995). The rate of SST change is caused by zonal advection (R_u), meridional advection (R_v), net interfacial heat flux (R_h), and horizontal diffusion (R_d). Note that the entrainment and net surface heat flux terms contain effects of the variable ML depth.

When the ML depth is a constant, (3.1) can be readily used to assess the contributions of the surface heat fluxes and ocean transport to the annual cycle of SST or ML heat content (e.g., Enfield 1986). If, however, the ML depth varies with time, use of (3.1) does not allow separation of the contributions of the ML depth variation from those due to the entrainment and surface heat fluxes. In addition, (3.1) is not suitable for analysis of the ML heat content. To circumvent these problems, we will use two diagnostic equations, one for the ML heat content and the other for the SST tendency in which the contribution of ML depth variation and those of entrainment and surface heat fluxes are separable.

The ML heat content equation can be derived by combining the continuity and thermodynamic equations. The ML depth, h_1, is governed by the continuity equation

$$\frac{\partial h_1}{\partial t} = -\nabla\cdot(h_1\mathbf{V}_1) + W_e + \nu\nabla^2(h_1), \tag{3.2}$$

where W_e represents the rate of entrainment (positive value) or detrainment (negative value). The last term on the right-hand side denotes horizontal diffusion. Multiplying (3.2) by $\rho_r C_w T_1$ and (3.1) by $\rho_r C_w h_1$, respectively, then taking the sum of the resulting equations, we obtain an equation for the ML heat content, $H = \rho_r C_w h_1 T_1$:

$$\frac{\partial H}{\partial t} = Q_u + Q_v + Q_{\text{ENT}} + Q_{\text{nsw}} + Q_{\text{lh}} + Q_{\text{sh}} + Q_{\text{lw}} + D, \tag{3.3}$$

where $D = \nu T_1\nabla^2 h_1 + \mu h_1\nabla^2 T_1$ is the heat content loss due to horizontal diffusion; the quantities

$$Q_u = -\frac{\partial}{\partial x}(u_1 H) \quad \text{and} \quad Q_v = -\frac{\partial}{\partial y}(v_1 H)$$

denote zonal and meridional component of the heat content convergence, respectively. The quantity

$$Q_{\text{ENT}} = Q_{\text{ent}} + \rho_r C_w T_1 W_e$$

represents the rate of heat content change associated with entrainment and detrainment. For an entraiment ($W_e > 0$), Q_{ENT} is positive, meaning that the ML heat content increases due to gain of water mass. On the other hand, if a detrainment occurs ($W_e < 0$), Q_{ENT} is negative, or the ML heat content decreases. The first two terms on the right-hand side of (3.3) express the effect of Ekman transport. Equation (3.3) can be used to study the ML heat content budget. According to (3.3), change of ML heat content is primarily caused by the Ekman transport (upwelling), entrainment, and the surface heat fluxes.

In order to separate the effect of ML depth variations from those of surface heat fluxes and entrainment, we consider the *rate of change of SST tendency*. A finite difference form for the change of SST tendency can be obtained by taking the finite difference of (3.1) with respect to time (central difference):

$$\Delta\left(\frac{\partial T_1}{\partial t}\right) = \Delta R_u + \Delta R_v + \Delta R_d + \frac{1}{\rho_r C_w h_1} \times \left[(\Delta Q_{\text{ent}} + \Delta Q_{\text{nsw}} + \Delta Q_{\text{lh}} + \Delta Q_{\text{sh}} + \Delta Q_{\text{lw}}) - \frac{\Delta h_1}{h_1}(Q_{\text{ent}} + Q_{\text{nsw}} + Q_{\text{lh}} + Q_{\text{sh}} + Q_{\text{lw}})\right], \tag{3.4}$$

where $\nabla(\partial T_1/\partial t) = (\partial T_1/\partial t)_{\text{May}} - (\partial T_1/\partial t)_{\text{March}}$ represents the change of SST tendency from March to May. Similarly, ΔQ_{ent}, ΔQ_{nsw}, ΔQ_{lh}, and Δh_1 denote, respectively, the changes in the entrainment flux, the net shortwave radiation flux, the latent heat flux, and the ML depth

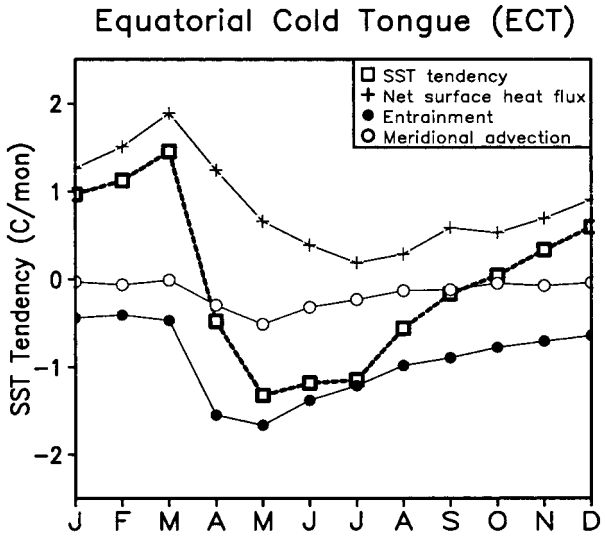

FIG. 5. The SST tendency (°C month^{-1}) budget over the equatorial cold tongue (4°S–2°N, 120°–90°W) in the control run. Shown are the total rate of SST change (dash line) and the major rhs terms in (3.1): entrainment, net surface heat flux, and meridional advection. The zonal advection and horizontal diffusion terms are negligibly small and are not shown.

from March to May. The first three terms on the right-hand side of (3.4) are, respectively, zonal advection, meridional advection, and dissipation. The terms, h_1, Q_{ent}, Q_{nsw}, Q_{lh} are assigned their corresponding April mean values in the study of boreal spring variability. Equation (3.4) indicates that the change of SST tendency is determined by changes in horizontal advection (ΔR_u and ΔR_v), surface heat fluxes (mainly ΔQ_{nsw}, ΔQ_{lh}), entrainment rate (ΔQ_{ent}), and the ML depth (Δh_1).

4. Mechanism of the annual reestablishment of the cold tongue

The rapid reestablishment of the ECT is signified by a drastic reversal of the warming trend from March to May. The thick dashed line in Fig. 5 shows the simulated monthly mean SST tendency (the rate of SST change averaged over 1 month). The annual warming (defined by a positive rate of SST change) occurs in October and reaches a maximum rate in March. Then, the warming abruptly turns into a cooling in April, followed by an annual maximum cooling rate occurring in May. The increase of SST tendency from May to the next March lasts 10 months, but the decrease of SST tendency takes only 2 months. From March to May, the SST tendency dramatically decreases from +1.5°C month^{-1} to −1.3°C month^{-1}. What processes are responsible for the sharp turnabout of the SST tendency in boreal spring?

a. The heat content budget in the ECT mixed layer

From March to May, the radiation and surface latent heat fluxes, which are received by the mixed layer, decrease rapidly. The net downward surface heat flux into the ECT calculated using (3.3) from the model simulation compares favorably with that derived from the Comprehensive Ocean–Atmosphere Data Set (COADS) by Oberhuber (1988) (Fig. 6a). Although the simulated net downward heat flux is systematically lower than its

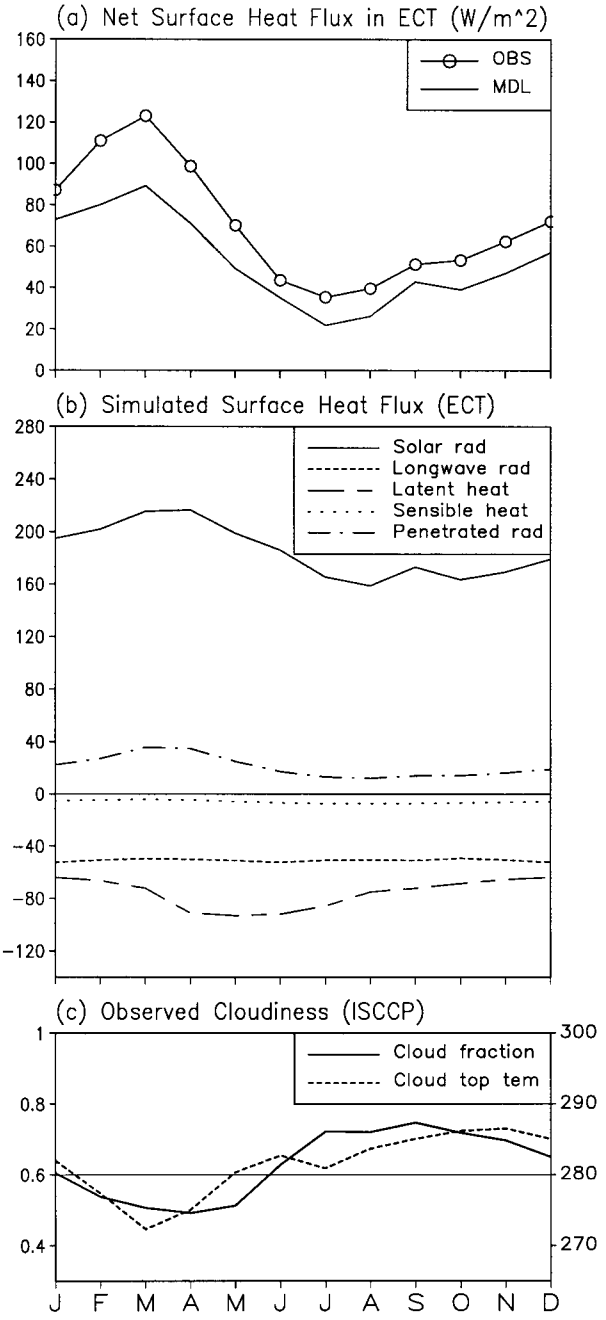

FIG. 6. Radiation and buoyancy flux budget in the equatorial cold tongue (ECT): (a) the observed (OBS) and simulated (MDL) annual variations of net surface heat fluxes, and (b) the simulated annual variations of surface heat flux components. (c) The observed cloud cover from ISCCP in the eastern equatorial Pacific (4°S–2°N, 120°–90°W).

observed counterpart by about 20–30 W m^{-2}, the simulated annual variation agrees well with observed variability with a maximum occurring in March and a minimum in July.

The individual components of the simulated downward surface heat fluxes shown in Fig. 6b indicate that from March to May the latent heat flux decreases (or the latent heat loss increases) by 21 W m^{-2} and the downward solar radiation flux decreases by 17 W m^{-2}. The latter is primarily due to the decrease of the solar declination angle, because the cloud fraction exhibits little change from March to May (Fig. 6c). Note that due to the deepening of the mixed layer, the solar radiation penetrating through the bottom of the mixed layer also decreases by 11 W m^{-2} (Fig. 6b). Therefore, the net reduction in the total amount of solar radiation absorbed by the mixed layer amounts to only 6 W m^{-2}. The reduction in the surface sensible heat flux and net longwave radiation is negligibly small (about 2 W m^{-2}). Therefore, from March to May, the total loss of buoyancy and radiation fluxes received by the mixed layer amounts to 29 W m^{-2}. These heat flux change terms are presented in the schematic diagram shown in Fig. 7a. The surface latent heat loss due to increased wind speeds accounts for the largest portion (76%). This indicates that the surface latent heat loss overwhelms all other components of the surface heat fluxes in the ML heat budget.

In comparison with the loss of radiation and surface buoyancy fluxes, the corresponding decrease of the heat flux due to entrainment is about 47 W m^{-2} and that due to meridional heat advection is 20 W m^{-2} (Fig. 7a). Therefore, from the point of view of the ML heat flux budget, the rapid decrease of the total heat flux received by a ML column from March to May is caused chiefly by the increased entrainment (47 W m^{-2}), followed by decreased net radiation and buoyancy fluxes (29 W m^{-2}) (primarily the surface latent heat loss) and meridional cold advection (20 W m^{-2}) (Fig. 7a). However, as shown in Fig. 7a, from March to May, the mixed layer deepens by about 7 m (or 40%), which is a critical factor influencing the ML heat content and temperature. In general, without taking into account the ML depth variation, the aforementioned heat flux budget cannot directly be used to deduce the causes of the changes in SST.

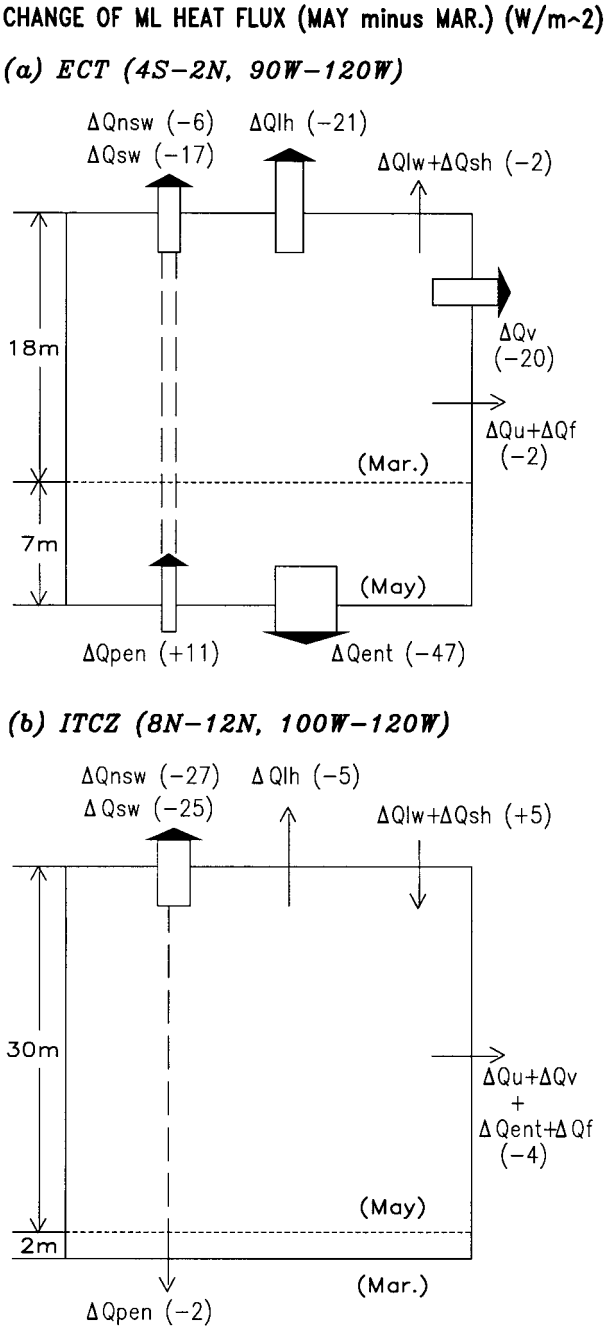

FIG. 7. Schematic diagrams showing the change of mixed layer heat fluxes (May minus Mar) for (a) the equatorial cold tongue (4°S–2°N, 90°–120°W), and (b) the ITCZ (8°–12°N, 100°–120°W).

b. SST tendency analysis

If we assess the contribution of the right-hand side terms of (3.1) to the rate of SST change, the total decrease of the SST tendency from March to May (−2.8°C month^{-1}) is mainly attributable to three processes: entrainment (−1.2°C month^{-1}), net surface heat exchange (−1.1°C month^{-1}), and meridional cold advection (−0.4°C month^{-1}; Fig. 5, Table 2). Note that the entrainment and the net surface heat flux terms in (3.1) contain the effect of the ML depth change. They represent the cooperative effects of the ML depth variation with the entrainment and net surface heat flux. Therefore, the dominant contributors to the initiation of the annual cooling of ECT, deduced from (3.1), are the combined effects of the ML deepening and enhanced entrainment, and the combined effects of the ML deepening and reduced surface heat fluxes. With the cooperative effect of ML depth variation, the contribution by the meridional cold advection is substantially re-

TABLE 2. Changes of SST tendency in the ECT from Mar to May computed using (3.1).

Rhs terms of (3.1)	Change of SST tendency (°C month^{-1})	Percentage change (%)
h_1[a] + Entrainment	−1.2	42.9
Meridional advection	−0.4	14.2
h_1 + net surface heat flux	−1.1	39.3
h_1 + latent heat flux	0	
h_1 + longwave radiation and sensible heat flux	+0.5	
h_1 + net solar radiation	−1.6	
Residuals[b]	−0.1	3.6
Total	−2.8	100

[a] h_1 represents the effects of varying mixed layer depth.
[b] Residuals include the terms of zonal advection and diffusion.

TABLE 3. Changes of the SST tendency (°C month^{-1}) in the ECT from Mar to May calculated from (3.4).

	h_1 (Apr)[a]		h_1 (mean)[a]	
Rhs terms of (3.4)	Change of SST tendency	Percentage (%)	Change of SST tendency	Percentage (%)
Entrainment	−1.5	53.5	−1.0	35.7
Meridional advection	−0.4	14.3	−0.4	14.3
Latent heat flux	−0.6	21.4	−0.5	17.8
Net solar radiation	−0.1	3.6	−0.1	3.6
Mixed layer deepening	−0.1	3.6	−0.7	25
Residuals[b]	−0.1	3.6	−0.1	3.6
Total	−2.8	100	−2.8	100

[a] h_1 (Apr) means that the Apr mean mixed layer depth is used, while h_1 (mean) indicates that the annual mean ML depth is used in (3.4).
[b] Residuals include the terms of zonal advection and diffusion, the longwave radiation, and sensible heat flux.

duced, and the contribution of the entrainment becomes comparable to that of the surface heat fluxes.

Note that inclusion of the effect of the ML depth variation also drastically changes the relative contributions of individual components of the surface heat fluxes (the net solar radiation, surface latent heat, net longwave radiation, and sensible heat flux). As shown in Fig. 7a, from March to May, the surface latent heat, the net solar radiation, and the longwave and sensible fluxes are reduced, respectively, by 21, 6, and 2 W m^{-2}. However, after including the effect of the ML depth variation, the contribution to the decrease of SST tendency from March to May due to the surface latent heat flux and net solar radiation are, respectively, zero and −1.6°C month^{-1}. The longwave radiation and sensible heat fluxes act to increase the rate of SST change (0.5°C month^{-1}, Table 2). The difference between the diagnostic results obtained using heat flux budget alone and using (3.1) is attributed to the ML depth variation. If, for example, the net solar radiation is fixed at 170 W m^{-2}, the deepening of the mixed layer from March to May would reduce the rate of SST change by −1.54°C month^{-1}. This suggests that the ML deepening changes substantially the relative contributions of the radiation and buoyancy fluxes.

In order to clarify the role of the ML deepening in changing the relative contributions of the entrainment, shortwave radiation, and buoyancy fluxes, we introduce a quantity measuring the efficiency of a heat flux component in changing the SST tendency (Fu 1998). Assume that Q_i denotes a heat flux component (e.g., entrainment heat flux, solar radiation) and R_i denotes the corresponding SST tendency induced by a heat flux, since $R_i = Q_i/(\rho_r C_w h_1)$ and the ML depth h_1 depends on Q_i, the change of SST tendency associated with a unit variation of the heat flux is

$$\frac{\partial R_i}{\partial Q_i} = \frac{1}{h_1}\left(\frac{1}{\rho_r C_w} - R_i \frac{\partial h_1}{\partial Q_i}\right). \tag{4.1}$$

Obviously, when h_1 varies with Q_i, the same amount of heat flux change does not necessarily cause the same amount of SST change. The calculation using (4.1) shows that the deepening of the ML during boreal spring reinforces the cooling efficiency of the decreased solar radiation by about eight times, whereas it reduces the cooling efficiency of the entrainment and latent heat flux, respectively, by about 30% and 130%, compared with those in a constant ML depth model.

The ML in the ECT is shallow in boreal spring and deep in fall (Fig. 2b). The sharp drop in the SST tendency during boreal spring is in part attributable to the spring shallowness of the ML. In order to elaborate on this point, we estimate the relative contributions of the entrainment, the net radiation, and buoyancy fluxes, and the meridional heat advection using (3.4), in which, for convenience of comparison, the mean ML depth takes two different values: the annual mean and the April mean. The results are compared in Table 3.

When the April mean ML depth is used, it is found that the rapid boreal spring cooling is primarily contributed to the turbulent entraiment (54%), surface evaporation (21%), and meridional advection (14%). The direct contribution of the mixed layer depth variation appears to be rather small (Table 3). The reason follows. As shown by the last term in (3.4), from March to May, the deepening of the ML combining with the entrainment and latent heat fluxes would result in a positive change of SST tendency, that is, reduces the cooling tendency. On the other hand, the deepening of the ML combining with the net shortwave radiation enhances the cooling trend. These assertions are consistent with those derived from (4.1). Because the deepening of the ML significantly reduces the contributions of the entrainment and latent heat fluxes, while it increases the contribution of the shortwave radiation, its net effect becomes small.

It should be pointed out that the effect of the spring ML shallowness is implicitly included in the increased contribution of the entrainment. Comparison of the two sets of results shown in Table 3 indicates that the spring shallowness of the ML increases the entrainment con-

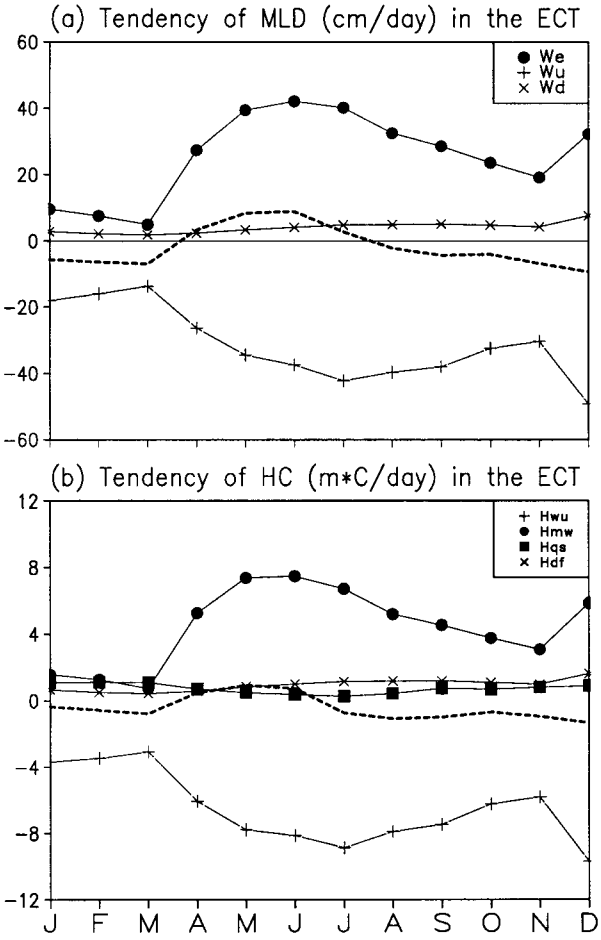

FIG. 8. (a) The ML depth tendency and (b) heat content tendency over the eastern equatorial Pacific (4°S–2°N, 120°–90°W) in the simulation. (a) The net rate of ML depth change (dash line) and the rhs terms in (3.2): upwelling (w_u), entrainment (w_e), and diffusion (w_d). (b) The net rate of heat content change (dash line) and the rhs terms in (3.3): upwelling ($H_{wu} = Q_u + Q_v$), entrainment ($H_{mw} = Q_{ENT}$), net surface heat flux ($H_{qs} = Q_{nsw} + Q_{lh} + Q_{sh} + Q_{lw}$), and diffusion ($H_{df} = D$).

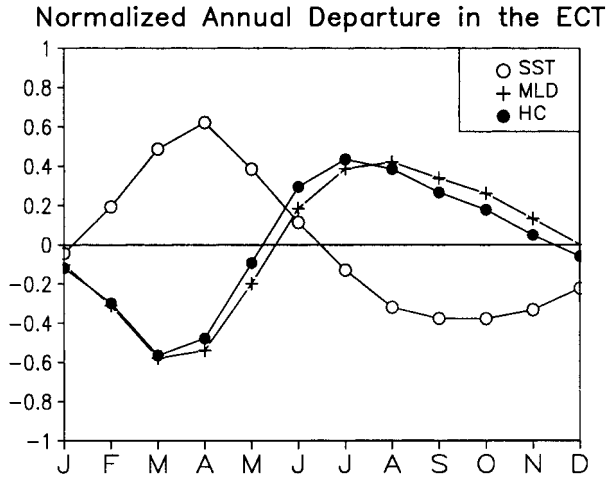

FIG. 9. The annual departure of SST (°C), the ML depth (MLD, m), and the ML heat content (HC, m °C) normalized by their corresponding annual range in the equatorial cold tongue of the eastern Pacific.

tribution from 35.7% to 53.5%. The differences between the results obtained using the annual mean and April mean ML depths implies that the annual variation of the ML depth contributes about 21% to the rapid decrease of the SST tendency in boreal spring. From the last column of Table 3, the primary processes contributing to the rapid reestablishment of the cold tongue from March to May are the entrainment, the annual variation of the mixed layer depth, the surface latent heat flux, and meridional heat advection.

5. Mechanism of the annual variation of the mixed layer depth

The SST tendency analysis reveals that the shallowness of the mixed layer in spring is an important factor for the rapid reestablishment of the ECT. What causes the spring shallowness of the ML? To answer this question, we use the diagnostic equation [(3.2)] to estimate the relative contributions of the Ekman divergence and the effects of entrainment and detrainment. Results are shown in Fig. 8a. The change of the ML depth is primarily determined by the divergence of the ML currents associated with Ekman flow (namely, upwelling) and the entrainment at the ML base due to turbulent mixing. The ML depth tendencies induced by upwelling and entrainment exhibit opposite signs and opposite tendencies of variation. Upwelling always tends to decrease the ML depth through poleward Ekman transport driven by the easterly trades (i.e., the zonal component of the surface winds). On the other hand, the entrainment associated with wind-induced stirring (i.e., both the zonal and meridional components of the surface winds) acts to deepen the ML. The magnitudes of both the upwelling and entrainment approach a minimum in March then increase from March to July following the intensification of the surface winds (Fig. 2d). The mixed layer shoals from August to the following March as the effect of upwelling surpasses that of entrainment. From March to August, in association with the rapid intensification of the surface winds (mainly the meridional cross-equatorial wind component), the entrainment impact surpasses that of upwelling, causing a ML deepening. Therefore, the variation of the ML depth results from the competing effects of entrainment and upwelling.

In the equatorial eastern Pacific, the annual variation of the ML depth is a good indicator of the annual variations of the ML heat content and SST (Fig. 9). The ML depth tends to vary in phase with the ML heat content and nearly 180° out of phase with that of the SST, albeit with a 1-month phase delay. On the interannual timescale, variations of SST and ML depth are positively correlated (Hayes et al. 1991). However, on

the annual timescale, variations of SST and the ML depth are negatively correlated. This suggests that fundamentally different mechanisms govern the SST variability of the ECT on annual and interannual timescales.

The nearly in-phase relationship between the ML depth and ML heat content suggests the dominant role of the ML depth variation in the annual cycle of the ML heat content. A ML heat budget analysis using the exact heat content [(3.3)] was carried out, and the results are presented in Fig. 8b. The dominant balance is between the entrainment and upwelling effects. These two large terms tend to cancel each other. The other terms are negligibly small. The resultant tendency of the ML heat content is small, and a positive tendency is associated with the entrainment effect exceeding that of upwelling. The processes governing the annual cycle of the ML heat content are essentially the same as those governing the annual cycle of the ML depth. Thus, it is reasonable to use ML depth variation to infer the annual variation of the ML heat content in the equatorial eastern Pacific.

6. Mechanism of the annual warming in the ITCZ and associated northward propagation

Under the ITCZ, the ocean mixed layer is about 50% deeper than it is in the ECT (Fig. 7). From March to May the ML shoals by about 2 m (7%). Therefore, the ML depth can be approximately treated as a constant. The changes of the heat fluxes received by the ML column are good indicators for SST variation.

In the vicinity of the ITCZ, the net surface heat flux simulated in the model agrees well with observations (Fig. 10a). From January to March, the increase of the net surface heat flux is primarily controlled by the surface solar radiation, whereas the latent heat flux hardly changes (Fig. 10b). The increase of solar radiation is due to the increased solar declination angle, as the local cloud cover is nearly unchanged (Fig. 10c). The net surface heat flux, and thus the warming rate, reach a maximum in March (in the model) and April (observation) and drop sharply in May due to increased cloudiness and enhanced evaporative cooling. In contrast to the ECT, the net surface heat flux variation is a dominant factor for the ML heat content and SST change in the ITCZ, while ocean dynamics play a minor role (Fig. 7b). The warming from March to May is primarily caused by the increased net surface heat flux.

The observed annual warming occurs progressively later northward in the eastern Pacific (Fig. 1a), which is reasonably reproduced by the present coupled model (Fig. 1e). What is responsible for this annual progression of warming? To seek the answer to this question, we examine the variation of SST tendency along 100°W. Figure 11 presents the right-hand-side terms of (3.1), which are responsible for the SST tendency as functions of calendar month and latitude. The northward progression of the spring warming in the Northern Hemisphere (Fig. 1e) is reflected in the annual variation of

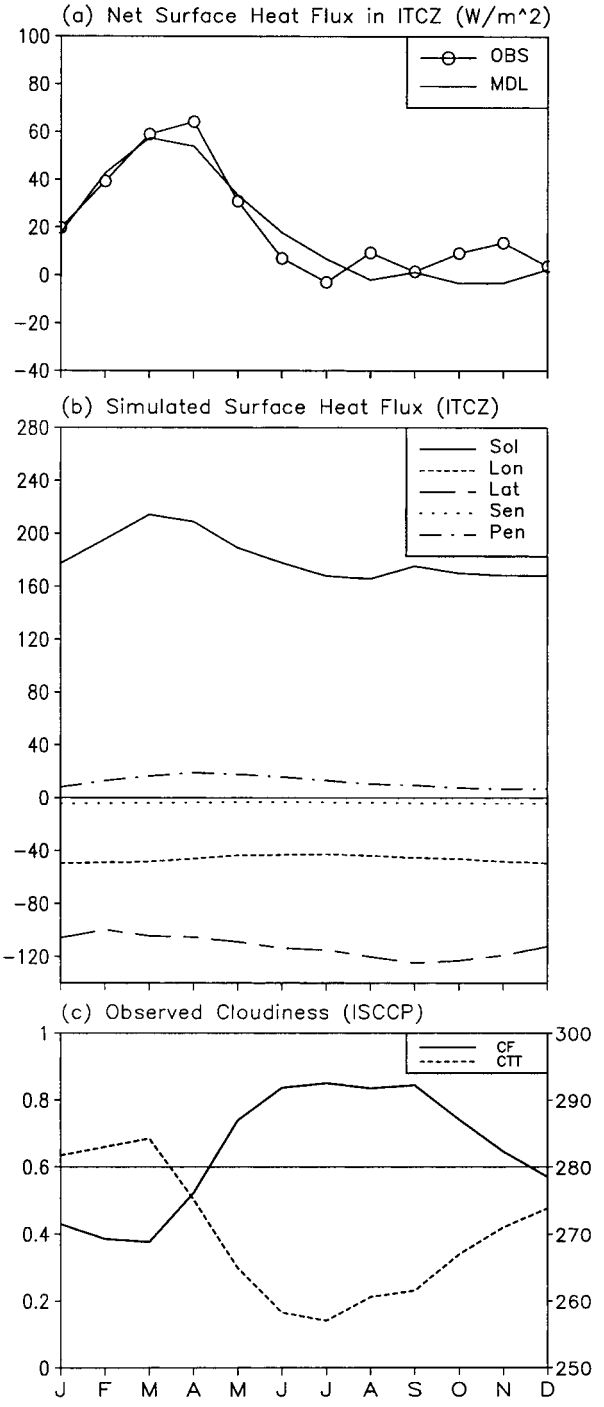

FIG. 10. Same as in Fig. 6, but for the ITCZ of the eastern Pacific.

the SST tendency (Fig. 11a). The maximum SST tendency occurs in March near the equator and in April between 10° and 15°N (Fig. 11a). In the region between 5°S and 5°N, all terms (i.e., the net surface heat flux, entrainment, and horizontal heat advection) have nonnegligible contributions to the rate of SST change. However, north of 5°N, the SST tendency is primarily con-

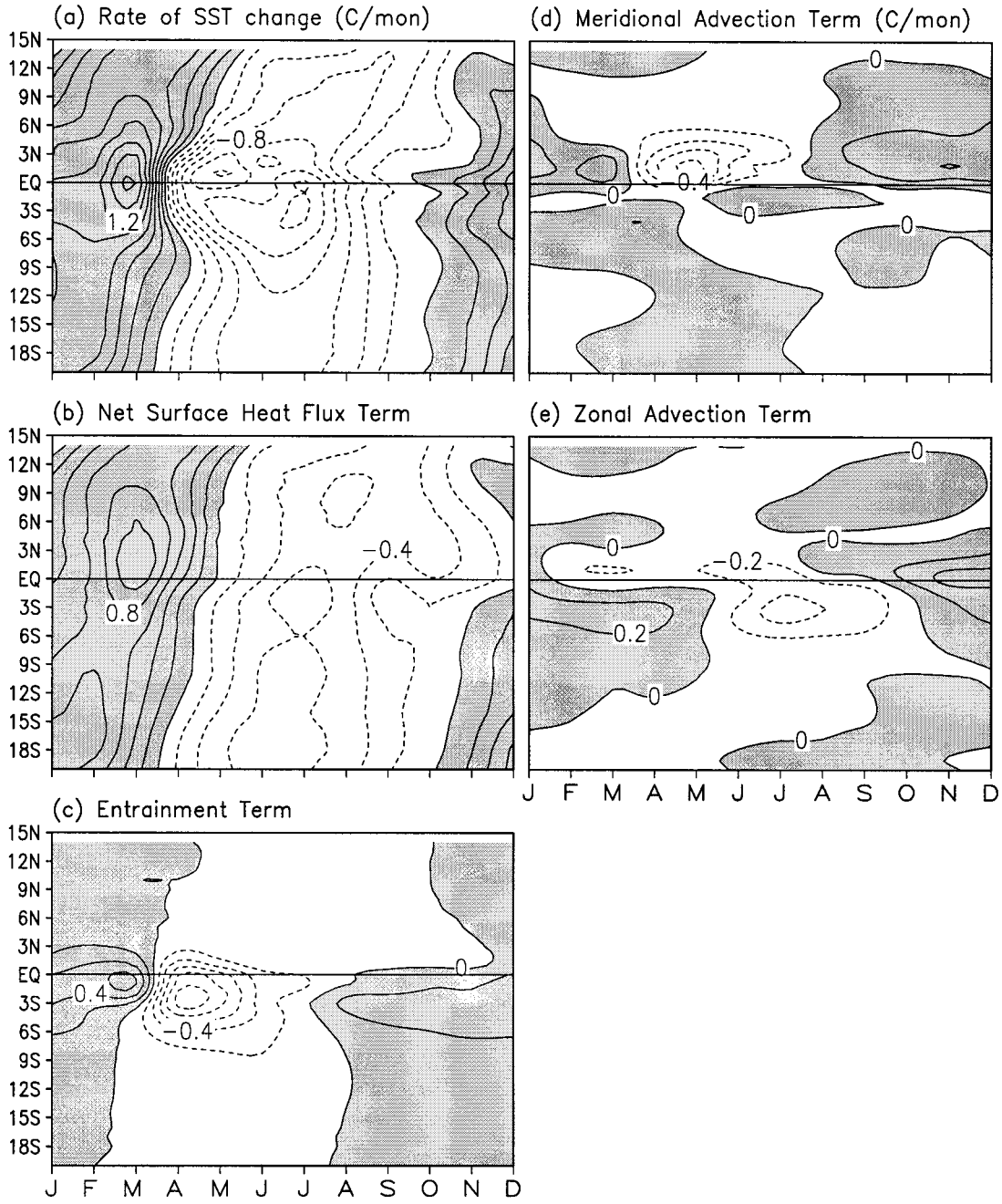

FIG. 11. The simulated annual perturbations along 100°W for (a) the rate of SST change (C month^{-1}) and the rhs terms in (3.1): (b) net heat flux, (c) entrainment, (d) meridional advection, and (e) zonal advection.

trolled by the net surface heat flux (Fig. 11b). The equatorial cooling from April to May is primarily caused by enhanced entrainment, latent heat flux and meridional cold advection (Figs. 11b–d). Therefore, the maximum SST occurs at least 1 month earlier than what can be accounted for by the net surface heat flux alone (Fig. 11b). It is the cooperative effects of the surface heat flux forcing and the concurrent equatorial cooling that result in the northward progression of the SST tendency.

To see what determines the net surface heat flux variability, we show, in Fig. 12, the annual variation of the dominant components of the surface heat fluxes along 100°W. Under a clear sky, the annual variation of the downward solar radiation along 100°W is shown in Fig. 12a. If the SST were primarily driven by the clear-sky solar radiation in the region north of 10°N where the maximum solar radiation occurs in May–July, the maximum SST would occur in August–October. This is the

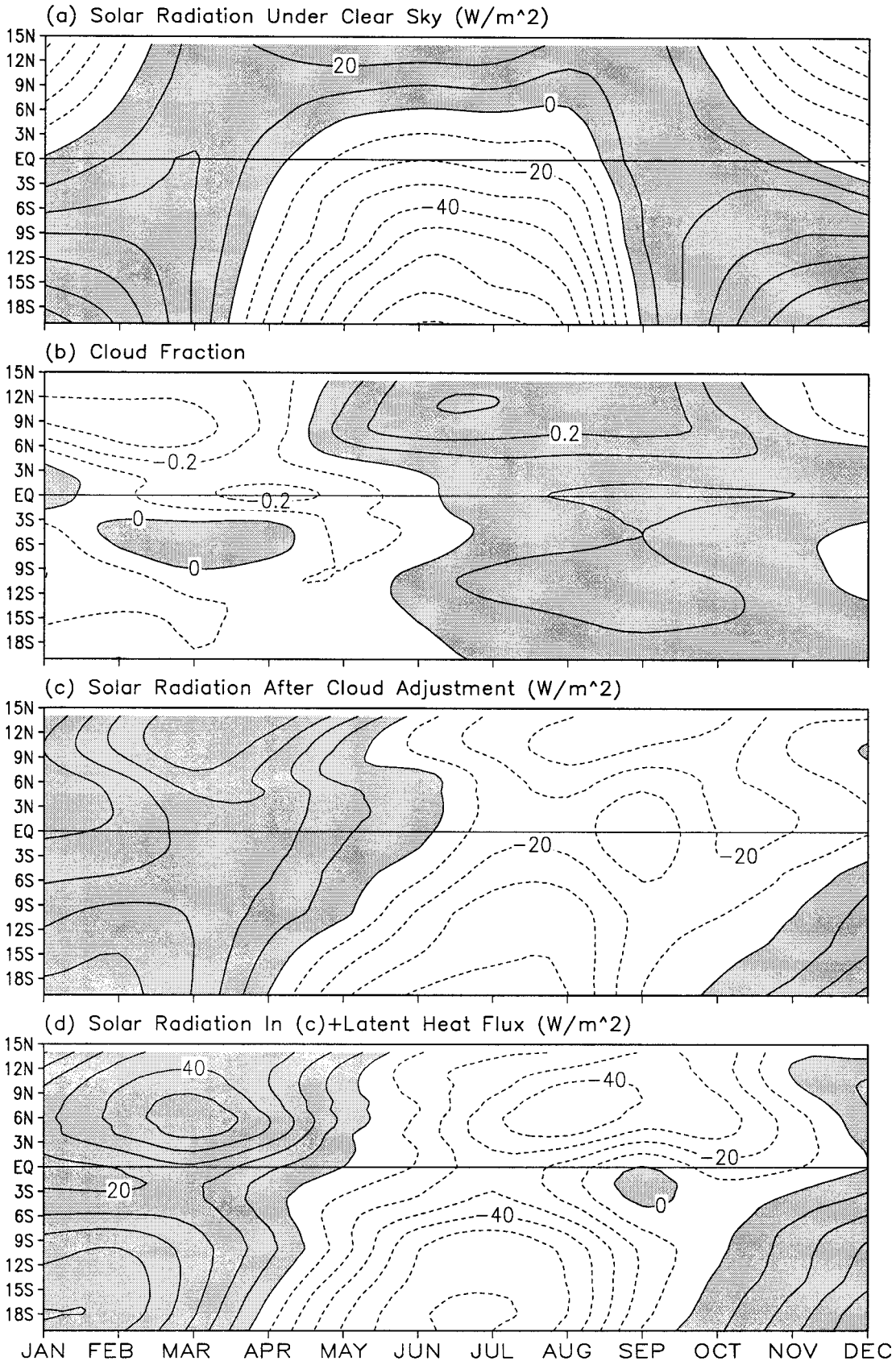
(a) Solar Radiation Under Clear Sky (W/m^2)
(b) Cloud Fraction
(c) Solar Radiation After Cloud Adjustment (W/m^2)
(d) Solar Radiation In (c)+Latent Heat Flux (W/m^2)
15N
12N
9N
6N
3N
EQ
3S
6S
9S
12S
15S
18S
JAN FEB MAR APR MAY JUN JUL AUG SEP OCT NOV DEC

case in the central and western Pacific (Liu and Xie 1994). However, in the eastern Pacific ITCZ region, the large-amplitude variation of the cloud cover (Fig. 12b) substantially modifies the downward solar radiation (Fig. 12c). North of 8°N, the downward solar radiation reaches a maximum in March and the maximum SST forced by this downward solar radiation should occur in June, about a season ahead of that under a clear sky. The sum of the downward solar radiation and surface latent heat fluxes exhibits an evident northward migration similar to that of the net surface heat fluxes (Fig. 12d). Comparison of Figs. 12c and 12d indicates that the reduced surface latent heat loss in March north of the equator causes an early occurrence of the maximum net surface downward heat flux. Results shown in Fig. 12d suggest that the northward progression in the annual perturbation of net surface heat flux is primarily caused by the modification of the cloud cover to the solar radiation flux and the surface latent heat flux.

7. Conclusions and discussion

In the eastern Pacific, the ITCZ–ECT complex exhibits abrupt development during boreal spring. Uncertainties in the available surface heat flux and wind stress observations have limited our capability to qualitatively assess the relative contributions of various physical processes to the annual variation of SST in this region. In this paper, we attempt to take a coupled ocean–atmosphere model approach to provide an alternative solution. The underlying premise is that the heat exchange between the ocean and atmosphere can be determined internally using a coupled system that reproduces realistic variability in both the ocean and atmosphere.

Since the mixed layer depth in the eastern equatorial Pacific has pronounced annual variation (Kessler et al. 1998; Swenson and Hanson 1999), it is imperative to deal with the effect of the seasonally varying mixed layer depth on SST. We used two diagnostic equations, one for the ML heat content and the other for the change of SST tendency. The former allows assessment of the contribution of individual fluxes to SST variation provided the ML depth is unchanged (as in the ITCZ case). The latter is a novel one dealing with the situation where the ML depth varies significantly (as in the ECT case). It has the advantage of separating the effects of the ML depth variation from those of entrainment and surface heat fluxes, overcoming the weakness of the traditional SST tendency equation [(3.1)].

Previous studies have suggested that upwelling and meridional cold advection in association with the cross equatorial wind are the primary mechanisms for the onset of the annual cooling in the ECT (e.g., Chang 1996; Li and Philander 1996). This conclusion is valid provided the mixed layer entrainment is negligibly small and the mixed layer depth is nearly constant. From March to May, the mixed layer in the cold tongue deepens from 18 to 25 m. This rapid deepening is accompanied by strong entrainment. In our coupled model, the rapid annual cooling of the ECT is primarily attributed to the turbulent entrainment (54%), surface evaporative cooling (21%), and meridional advection (14%). The boreal spring shallowness of the mixed layer contributes to the rapid cooling implicitly through reinforcing the effects of the entrainment. From March to May, the ML deepens by about 35%. This deepening enhances the cooling due to reduction in the solar radiation, but decreases the cooling efficiency of the evaporation and entraiment. Thus, the net contribution of the ML deepening turns out to be small. The results of this study indicate that improvement of the modeling of mixed layer entrainment and thermodynamics holds the key to accurate simulation of the annual cycle of the equatorial eastern Pacific cold tongue.

The annual variation of the ML depth is determined by the competing effects of upwelling and entrainment. Upwelling tends to decrease the ML depth through poleward Ekman transport driven by the zonal wind stress at the equator. On the other hand, entrainment is associated with wind-induced stirring effects, and is sensitive to wind speed variations in both the zonal and meridional components. From March to July, the effect of entrainment surpasses that of upwelling, resulting in a deepening of the mixed layer. Although both the zonal and meridional winds increase, the meridional wind increase is nearly twice as large as that of the zonal wind (Figs. 1b and 1c). The strengthening of entrainment is thereby favored. The mixed layer shoals from August through the following March due to the impact of upwelling overtaking that of entrainment.

In the eastern Pacific ITCZ, the spring warming is primarily attributable to surface heat fluxes, while entrainment and oceanic thermal advection play minor roles. Along 100°W, the maximum SST occurs in March at the equator, and progressively later northward, reaching a warm peak in the ITCZ during May. This northward progression of the annual SST perturbation arises from the surface shortwave and latent heat flux forcing and concurrent equatorial cooling.

It should be noted that the present heat budget analysis aims to sort out the contributions of various processes to the ML heat budget and SST variation. This ocean-centered view considers the atmospheric forcing being given. In reality, the atmospheric forcing is af-

←

FIG. 12. The annual perturbations of the solar radiation (W m^{-2}) under (a) clear sky, (b) the observed cloud fraction (ISCCP), and (c) the downward solar radiation reaching the ocean surface (W m^{-2}) and (d) the downward solar radiation in (c) plus latent heat flux (W m^{-2}) along 100°W.

fected by SST. Therefore, air–sea interaction is actively involved in the annual variation of the ITCZ–ECT complex. For instance, the downward shortwave radiation shows a clear northward progression due to modulation of shortwave radiation by cloud cover in the ITCZ. Since the cloud amount in the ITCZ depends on surface wind convergence, which is, in turn, affected by SST gradients in the boundary layer, we should view this northward propagation of annual warming as a result of the ITCZ–ECT interaction (Mitchell and Wallace 1992; Wang and Wang 1999). In April, with the intensification of the surface southerly wind, the convection and cloud cover in the ITCZ are enhanced due to increased moisture convergence. The increased cloud cover blocks incoming solar radiation, further limiting the increase of SST and resulting in occurrence of the maximum SST in May–June, which is about one season ahead of what the seasonal march of the solar radiation can account for. At the same time, the increased surface winds near the equator strengthen entrainment, the surface latent heat flux, and cold meridional advection. All of these processes, working together, cool the equatorial ocean and lead to a sharp turnabout the warming trend at the equator. The important role of the wind–evaporation feedback in the eastern Pacific annual cycle was previously emphasized by Xie and Philander (1994), Liu and Xie (1994), and Liu (1996). The results of this study suggest that coupled ocean–atmosphere models are required to accurately simulate the annual cycle of the ITCZ–ECT complex.

In this study, we have focused on the oceanic processes of the air–sea coupling system and suggested the importance of entrainment, mixed layer depth variation, and latent heat flux on the rapid annual reestablishment of the eastern Pacific cold tongue. Most of these processes are associated with the intensification of the southeast trades. It has been proposed that the intensification of the southeast trades over the eastern Pacific is caused by multiple processes, including antisymmetric solar forcing (the contrast in the solar forcing in the Northern and Southern Hemispheres; Wang 1994), atmosphere–ocean–land interaction (Philander et al. 1996; Li and Philander 1997), and the seasonal variation of the ML depth on the air–sea interaction. Note also that the annual variations of the clouds in the present coupled model are prescribed. The extent to which interactive clouds might change the results presented here is unknown, but potentially important, especially the stratus cloud–radiation–SST feedback (Philander et al. 1996). In order to address this question, a fully coupled model is needed. We are currently using such a model to further our understanding of the ITCZ–ECT complex.

Acknowledgments. The present work has been supported by the NOAA Pan-American Climate Study (PACS). The authors thank Dr. S. Kemball-Cook for comments on an earlier version of the manuscript. This is School of Ocean and Earth Science and Technology publication number 5354 and International Pacific Research Center publication number 80. The International Pacific Research Center is partly sponsored by the Frontier Research System for Global Change.

REFERENCES

Chang, P., 1996: The role of the dynamic ocean–atmosphere interactions in the tropical seasonal cycle. *J. Climate,* **9,** 2973–2998.

——, and S. G. Philander, 1994: A coupled ocean–atmosphere instability of relevance to seasonal cycle. *J. Atmos. Sci.,* **51,** 3627–3648.

Chen, D., A. J. Busalacchi, and L. M. Rothstein, 1994: The roles of vertical mixing, solar radiation and wind stress in a model simulation of the sea surface temperature seasonal cycle in the tropical Pacific Ocean. *J. Geophys. Res.,* **99** (C10), 20 345–20 359.

Enfield, D. B., 1986: Zonal and seasonal variations in the near surface heat balance of the equatorial ocean. *J. Phys. Oceanogr.,* **16,** 1038–1054.

Fu, X., 1998: Simulation of the tropical Pacific annual cycle with an intermediate ocean–atmosphere–land model. Ph.D. dissertation, University of Hawaii at Manoa, 228 pp.

——, and B. Wang, 1999: The role of longwave radiation and boundary layer thermodynamics in forcing tropical surface winds. *J. Climate,* **12,** 1049–1069.

——, and ——, 2001: A coupled modeling study of the seasonal cycle of the Pacific cold tongue. Part I: Simulation and sensitivity experiments. *J. Climate,* **14,** 765–779.

Gaspar, P., 1988: Modeling the seasonal cycle of the upper ocean. *J. Phys. Oceanogr.,* **18,** 161–180.

Hayes, S. P., P. Chang, M. J. McPhaden, 1991: Variability of the sea surface temperature in the eastern equatorial Pacific during 1986–1988. *J. Geophys. Res.,* **96,** 10 553–10 566.

Ji, M., A. Leetmaa, and J. Derber, 1995: An ocean analysis system for seasonal to interannual climate studies. *Mon. Wea. Rev.,* **123,** 460–481.

Kessler, W. S., L. M. Rothstein, and D. Chen, 1998: The annual cycle of SST in the eastern tropical Pacific, diagnosed in an ocean GCM. *J. Climate,* **11,** 777–799.

Li, T., and S. G. H. Philander, 1996: On the annual cycle of the eastern equatorial Pacific. *J. Climate,* **9,** 2986–2997.

——, and ——, 1997: On the seasonal cycle of the equatorial Atlantic. *J. Climate,* **10,** 813–817.

Liu, Z. Y., 1996: Modeling equatorial annual cycle with a linear coupled model. *J. Climate,* **9,** 2376–2385.

——, and S. P. Xie, 1994: Equatorial propagation of coupled air–sea disturbances with application to the annual cycle of the eastern tropical Pacific. *J. Atmos. Sci.,* **51,** 3807–3822.

McPhaden, M. J., 1982: Variability in the central equatorial Indian Ocean. Part II: Oceanic heat and turbulent energy balance. *J. Mar. Res.,* **40,** 403–419.

Mitchell, T. P., and J. M. Wallace, 1992: On the annual cycle in equatorial convection and sea-surface temperature. *J. Climate,* **5,** 1140–1156.

Murakami, T., B. Wang, and S. W. Lyons, 1992: Summer monsoons over the Bay of Bengal and the eastern North Pacific. *J. Meteor. Soc. Japan,* **70,** 191–210.

Oberhuber, J. M., 1988: An atlas based on the COADS data set: The budgets of heat, buoyancy and turbulent kinetic energy at the surface of the global ocean. Max-Planck-Institut für Meteorologie Rep. No. 15, Hamburg, Germany, 20 pp + plates.

Philander, S. G. H., and Coauthors, 1996: Why the ITCZ is mostly north of the equator. *J. Climate,* **9,** 2958–2972.

Sadler, J. C., M. A. Lander, A. M. Hori, and L. K. Oda, 1987: *Tropical Marine Climate Atlas.* Report UHMET 87-02, Department of Meteorology, University of Hawaii, Honolulu, HI.

Swenson, M. S., and D. V. Hanson, 1999: Tropical Pacific Ocean

mixed layer heat budget: The Pacific cold tongue. *J. Phys. Oceanogr.*, **29,** 69–81.

Wang, B., 1994: On the annual cycle in the tropical eastern central Pacific. *J. Climate,* **7,** 1926–1942.

——, and T. Li, 1993: A simple tropical model of relevance to short-term climate variations. *J. Atmos. Sci.,* **50,** 260–284.

——, ——, and P. Chang, 1995: An intermediate model of the tropical Pacific Ocean. *J. Phys. Oceanogr.,* **25,** 1599–1616.

——, and Y. Wang, 1999: Dynamics of the ITCZ–equatorial cold tongue complex and causes of the latitudinal climate asymmetry. *J. Climate,* **12,** 1830–1847.

Xie, P. P., and P. A. Arkin, 1996: Analyses of global monthly precipitation using gauge observations, satellite estimates, and numerical model predictions. *J. Climate,* **9,** 840–858.

Xie, S., and G. Philander, 1994: A coupled ocean–atmosphere model of relevance to the ITCZ in the eastern Pacific. *Tellus,* **46A,** 340–350.

Yu, X., and M. J. McPhaden, 1999: Seasonal variability in the equatorial Pacific. *J. Phys. Oceanogr.,* **29,** 925–947.